Article

Stable (Long-Bonded) Dimers via the Quantitative Self-Association of Different Cationic, Anionic, and Uncharged -Radicals: Structures, Energetics, and Optical Transitions

Jian-Ming L, Sergiy V. Rosokha, and Jay K. Kochi

J. Am. Chem. Soc., **2003**, 125 (40), 12161-12171• DOI: 10.1021/ja0364928 • Publication Date (Web): 13 September 2003

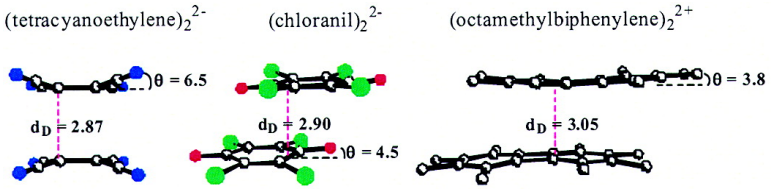

More About This Article

Additional resources and features associated with this article are available within the HTML version:

- Supporting Information
- Links to the 28 articles that cite this article, as of the time of this article download
- Access to high resolution figures
- Links to articles and content related to this article
- Copyright permission to reproduce figures and/or text from this article

View the Full Text HTML

J|A|C|S
ARTICLES
Published on Web 09/13/2003

Stable (Long-Bonded) Dimers via the Quantitative Self-Association of Different Cationic, Anionic, and Uncharged π-Radicals: Structures, Energetics, and Optical Transitions

Jian-Ming Lü, Sergiy V. Rosokha, and Jay K. Kochi*

Contribution from the Department of Chemistry, University of Houston, Houston, Texas 77204-5003

Received June 3, 2003; E-mail: jkochi@uh.edu

Abstract: Unusual dimers with wide interplanar separations, that is, very long bonds with $d_D \approx 3.05$ Å, are common to the spontaneous self-association of various organic π-radicals in solution and in the crystalline solid state, independent of whether they are derived from negatively charged anion radicals of planar electron acceptors (**TCNE**$^{-\bullet}$, **TCNQ**$^{-\bullet}$, **DDQ**$^{-\bullet}$, **CA**$^{-\bullet}$), positively charged biphenylene cation-radical (**OMB**$^{+\bullet}$), or neutral phenalene radical (**PHEN**$^{\bullet}$). All dimeric species are characterized by intense absorption bands in the near-IR region that are diagnostic of the charge-transfer transitions previously identified with intermolecular associations of various electron-donor/acceptor dyads. The extensive delocalizations of a pair of π-electrons accord with the sizable values of (i) the enthalpies ($-\Delta H_D$) and entropies ($-\Delta S_D$) of π-dimerization measured by quantitative UV−vis/EPR spectroscopies and (ii) the electronic coupling element H_{ab} evaluated from the strongly allowed optical transitions, irrespective of whether the diamagnetic dimeric species bear a double-negative charge as in (**TCNE**)$_2^{2-}$, (**TCNQ**)$_2^{2-}$, (**DDQ**)$_2^{2-}$, (**CA**)$_2^{2-}$ or a double-positive charge as in (**OMB**)$_2^{2+}$ or are uncharged as in (**PHEN**)$_2$. These long-bonded dimers persist in solution as well as in the solid state and suffer only minor perturbations with $\Delta d_D < 10\%$ from extra-dimer forces that may be imposed by counterion electrostatics, crystal packing, and so forth. The characteristic optical transitions in such diamagnetic two-electron dimers are shown to be related to those in the corresponding paramagnetic one-electron pimers of the same π-radicals with their parent acceptor, both in general accord with Mulliken theory.

Introduction

The spontaneous diffusion-controlled or "barrierless" second-order dimerization to form a new σ-bond is the distinguishing characteristic of the dynamic behavior of many organic and organometallic free radicals,[1] irrespective of whether the semioccupied orbital (SOMO) is centered on carbon or heteroatom. There is, however, experimental evidence in the extant solid-state literature[2] that some organic radicals lead to π-bonded as opposed to σ-bonded dimers in which the intermolecular separation of the fragments in the dimeric product is substantially longer than the conventional distance in a covalent bond.[3,4]

Chart 1

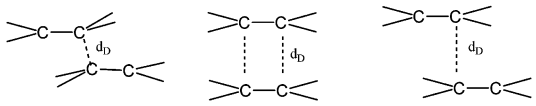

I II III

For example, the persistent tetracyanoethylene anion radical forms three types of dimeric products in the solid state (Chart 1), in which the intermolecular separation (d_D) in the σ-bonded dimer I is 1.61 Å compared to 2.90 Å and 3.47 Å in the π-bonded isomers II and III.[5] The exceptionally long C−C bonds in the dimeric structure II has been assigned by Novoa, Miller, and co-workers[4] to unusual two-electron four-center $\pi^*-\pi^*$ bonding, in which the attractive forces arising from positively charged counterions effectively offset the inherent electrostatic repulsion of two **TCNE**$^{-\bullet}$ moieties.[4] Otherwise, they showed[4,5] by ab initio MO computations that no clearly defined other than local, metastable energy minima could be identified in the absence of the counterion, and essentially the same electrostatics and bonding interactions may be qualitatively applied to the dimeric structure III.

(1) (a) Ingold, K. U. In *Free radicals*; Kochi, J. K., Ed.; Wiley: NY, 1973; Vol. 1, p 39 ff. (b) Benson, S. W. *Adv. Photochem.* **1964**, *2*, 1. (c) Trogler, W. C., Ed. *Organometallic Radical Processes*; Elsevier: NY, 1990.
(2) (a) Soos, Z. G.; Klein, D. J. In *Molecular Association*; Foster, R., Ed.; Academic: NY, 1975; Vol. 1. (b) Konno, M.; Saito, Y. *Acta Crystallogr.* **1974**, *B30*, 1294. (c) Miller, J. S., Ed. *Extended Linear Chain Compounds*; Plenum Press: NY, 1983; Vols. 2 and 3. (d) Zanotti, G.; Del Pra, A.; Bozio, R. *Acta Crystallogr.* **1982**, *B38*, 1225. (e) Vazquez, C.; Calabrese, J. C.; Dixon, D. A.; Miller, J. S. *J. Org. Chem.* **1993**, *58*, 65. (f) Johnson, M. T.; Arif, A. M.; Miller, J. S. *Eur. J. Inorg. Chem.* **2000**, 1781. (g) Novoa, J. J.; Lafuente, P.; Del Sesto, R. E.; Miller, J. S. *Cryst. Eng. Comm.* **2002**, *4*, 373. (h) Awere, E. G.; Burford, N.; Haddon, R. C.; Parsons S.; Passmore, J.; Waszczak, J. V.; White, P. S. *Inorg. Chem.* **1990**, *29*, 4821.
(3) (a) Gundel, D.; Sixl, H.; Metzger, R. M.; Heimer, N. E.; Harms, R. H.; Keller, H. J.; Nothe, D.; Wehe, D. *J. Chem. Phys.* **1983**, *79*, 3678. (b) Grossel, M. C.; Weston S. C. *Chem. Mater.* **1996**, *8*, 977 and references therein.
(4) Novoa, J. J.; Lafuente, P.; Del Sesto, R. E.; Miller, J. S. *Angew. Chem., Int. Ed.* **2001**, *40*, 2540.
(5) Del Sesto, R. E.; Miller, J. S.; Lafuente, P.; Novoa, J. *Chem.—Eur. J.* **2002**, *8*, 4894.

Chart 2

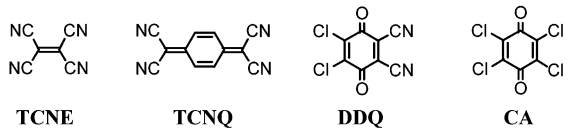

Solid-state EPR studies confirm the diamagnetic character of the **TCNE**$^{-\bullet}$ dimers;[5,6] and, spin-paired (singlet) ground states are also observed in crystalline salts of the anion-radical salts derived from the related electron acceptor tetracyanoquinodimethane[3a,7] (Chart 2) as well as its tetrafluoro derivative.[8]

Moreover, the same applies to quinonoid acceptors such as dicyanodichlorobenzoquinone,[9] which also readily yields a similar dimeric salt with a very large intermolecular separation of $d_D = 2.9$ Å.[2b,10] Most importantly, related crystalline dimers are obtained from the uncharged phenalene radical **PHEN**$^{\bullet}$ (Chart 3), and the positively charged octamethylbiphenylene cation-radical **OMB**$^{+\bullet}$ in which the long interplanar distances of $d_D = 3.2$ Å are substantially less than the van der Waals separation of 3.5 Å.[11,12] Electrostatic contributions of the counterion to dimer formation in these radicals are either nonexistent (**PHEN**$^{\bullet}$) or, in the case of **OMB**$^{+\bullet}$, minimally attractive owing to the very poor coordination to the large negatively charged $SbCl_6^-$ counterion.

Chart 3

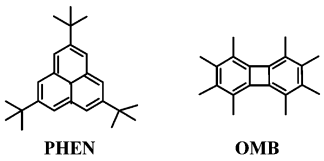

Since solid-state structures can be subject to different crystal-packing forces, it is not always clear how bimolecular interactions such as those leading to π-dimerizations, as reflected by X-ray crystallographic analyses, are related to those important in solution processes. Conversely, the binding interactions established in solution can provide valuable insight into those properties operating in extended systems characteristic of the solid state.[13] Heretofore, the π-dimerizations of neutral, anion, and cation radicals as briefly outlined above are singularly lacking in the quantitative coherency of the scattered published data for solid-state *vis à vis* solution studies. For example, the solid-state analyses of the different **TCNE**$^{-\bullet}$ dimers in Chart 1 lack experimental energies of intermolecular interactions, especially of counterion effects, which can be readily and unambiguously evaluated in solution. On the other hand, spectral studies of the dimerization in solution[14,15] have left open the critical question as to the nature of the dimer formed (σ- or π-bonded). Accordingly, our primary task in this comprehensive study is to isolate the primary bimolecular interaction for the unique π-dimerization process *in solution* by identifying the role of electrical charge in (a) the comparative behavior of the neutral uncharged radical (**PHEN**$^{\bullet}$) relative to its cationic (**OMB**$^{+\bullet}$) and anionic counterparts (**TCNE**$^{-\bullet}$, **TCNQ**$^{-\bullet}$, **DDQ**$^{-\bullet}$, and **CA**$^{-\bullet}$) and (b) the ion-pairing effects of the associated counterions on the π-dimerization of anion radicals in solution and in the solid state. We will focus on the temperature-dependent EPR and electronic UV−vis spectra of π-radical pairs since these lead to quantitative measures of the thermodynamic changes in their reversible dimerization. Furthermore, the characteristic optical transitions in π-bonded dimers are directly comparable to the charge-transfer absorption band in analogous intermolecular complexes previously identified as paramagnetic "pimers" of the same π-radicals with the parent acceptor.[16−18]

Results

I. Reversible Associations of π-Radicals in Solution. The positively charged biphenylene cation-radical **OMB**$^{+\bullet}$ in dichloromethane solution undergoes spontaneous dimerization in common with the uncharged phenylene π-radical **PHEN**$^{\bullet}$ counterpart in Chart 3, together with the anion radicals and the π-acceptors in Chart 2, the quantitative aspects of which were measured in the following way.

A. Diagnostic Electronic (UV−vis) Spectra of π-Bonded Dimers. The dimerization of the positively charged **OMB**$^{+\bullet}$,

(6) Johnson, M. T.; Campana, C. F.; Foxman, B. M.; Desmarais, W.; Vela, M. J.; Miller, J. S. *Chem.—Eur. J.* **2000**, *6*, 1805.
(7) (a) Miller, J. S.; Zhang, J. H.; Reiff, W. M.; Dixon, D. A.; Preston, L. D.; Reis, A. H., Jr.; Gebert, E.; Extine, M.; Troup, J.; Epstein, A.; Ward, M. D. *J. Phys. Chem.* **1987**, *91*, 4344. (b) Chesnut, D. B.; Phillips, W. D. *J. Chem. Phys*. **1961**, *35*, 1002.
(8) Metzger, R. M.; Heimer, N. E.; Gundel, D.; Sixl, H.; Harms, R. H.; Keller, H. J.; Nothe, D.; Wehe, D. *J. Chem. Phys.* **1982**, *77*, 6203.
(9) (a) Miller, J. S.; Krusic, P. J.; Dixon, D. A.; Reiff, W. M.; Zhang, J. H.; Anderson E. C.; Epstein, A. J. *J. Am. Chem. Soc.* **1986**, *108*, 4459. (b) Pasimeni, L.; Brustolon, M.; Zanonato, P. L.; Corvaja, C. *Chem. Phys.* **1980**, *51*, 381.
(10) (a) Yan, Y.-K.; Mingos, M. P.; Muller, T. E.; Williams, T. E.; Kurmoo, M. *J. Chem. Soc., Dalton Trans* **1995**, 2509. (b) Marzotto, A.; Clemente, D. A.; Pasimeni, L. *J. Crystallogr. Spectrosc. Res.* **1988**, *18*, 545.
(11) (a) Goto, K.; Kubo, T.; Yamamoto, K.; Nakasuji, K.; Sato, K.; Shiomi, D.; Takui, T.; Kubota, M, Kobayashi, T.; Yakushi, K.; Ouyang, J. *J. Am. Chem. Soc.* **1999**, *121*, 1619. (b) Fukui, K.; Sato, K.; Shiomi, D.; Takui, T.; Itoh, K.; Gotoh, K.; Kubo, T.; Yamamoto, K.; Nakasuji, K.; Naito, A. *Synth. Met.* **1999**, *103*, 2257. (c) The four (unique) protons were unresolved within the line widths.
(12) (a) Kochi, J. K.; Rathore, R.; Le Magueres, P. *J. Org. Chem*. **2000**, *65*, 6826. Note that the proton splittings of the four methyl groups at the 2, 3, 5, and 6 positions are unresolved. (b) In this paper, the X-ray structure (Figure 3) of the biphenylene dimer (**OMB**)$_2^{2+}$ was conceived as the rather close self-association of a pair of **OMB**$^{+\bullet}$ cation radicals; the X-ray structure (Figure 4) of the paramagnetic associate (**OMB**)$_2^{+\bullet}$ was then referred to as the *dimer(ic)* cation radical in accord with convention. However, to avoid any further ambiguity,[12c] the latter will be consistently designated hereinafter as the *pimer*. (c) Note that the term "pimer" was first employed by Kosower[12d] to designate what is now described herein as the "dimer"! (d) See: Kosower, E. M.; Hajdu, J. *J. Am. Chem. Soc.* **1971**, *93*, 2534.
(13) (a) Miller, L. L.; Mann, K. R. *Acc. Chem. Res.* **1996**, *29*, 417. (b) Graf, D. D.; Duan, R. G.; Campbell, J. P.; Miller, L. L.; Mann, K. R. *Am. Chem. Soc.* **1997**, *119*, 5888. (c) Penneau, J. F.; Stallman, B. J.; Kasai, P. H.; Miller, L. L. *Chem. Mater*. **1991**, *3*, 791. (d) Hubig, S. M.; Kochi, J. K. *J. Phys. Chem.* **1995**, *99*, 17578.
(14) (a) Hausser, K. H.; Murrell, J. N. *J. Chem. Phys.* **1957**, *27*, 500. (b) Boyd, R. H.; Phillips, *J. Chem. Phys*. **1965**, *43*, 2927. (c) Itoh, M. *Bull. Chem. Soc. Jpn.* **1972**, *45*, 1947. (d) Chang, R. *J. Phys. Chem.* **1970**, *74*, *2029*. (e) Yamagishi, A. *Bull. Chem. Soc. Jpn.* **1975**, *48*, 2440. (f) Bieber, A.; Andre, J. J. *Chem. Phys*. **1975**, *7*, 137. (g) Nakayama S.; Suzuki, K. *Bull. Chem. Soc. Jpn.* **1973**, *46*, 3694. (h) Kimura, M.; Yamada, H.; Tsubomura, H. *J. Chem. Phys*. **1968**, *48*, 440. (i) Itoh, M.; Nagakura, S. *J. Am. Chem. Soc.* **1967**, *89*, 3959. (j) Kosower, E. M.; Cotter, J. L. *J. Am. Chem. Soc.* **1964**, *86*, 5524. (k) Sakai, N.; Shirotani, I.; Minomura, S. *Bull. Chem. Soc. Jpn.* **1971**, *44*, 675. (l) Yu, Y.; Gunic, E.; Zinger, B.; Miller, L. L. *J. Am. Chem. Soc.* **1996**, *118*, 1013. (m) Hill, M. G.; Mann, K. R.; Miller, L. L.; Penneau, J.-F. *J. Am. Chem. Soc.* **1992**, *114*, 2728. (n) Hill, M. G.; Penneau, J. F.; Zinger, B.; Mann, K. R.; Miller, L. L. *Chem. Mater*. **1992**, *4*, 1106. (o) Levillain, E.; Ronkali, J. *J. Am. Chem. Soc.* **1999**, *121*, 8760.
(15) (a) Kawamori, A.; Honda, A.; Joo, N.; Suzuki, K.; Ooshika, Y. *J. Chem. Phys.* **1966**, *44*, 4363. (b) Evans, A. G.; Evans, J. C.; Baker, M. W. *J. Chem. Soc., Perkin Trans. 2* **1975**, 1310. (c) Evans, A. G.; Evans, J. C.; Baker, M. W. *J. Am. Chem. Soc.* **1977**, *99*, 5882. (d) Evans, A. G.; Evans, J. C.; Baker, M. W. *J. Chem. Soc., Perkin Trans. 2* **1977**, 1787. (e) Fairhurst, S. A.; Stewart, N. J.; Sutcliffe, L. H. *Magn. Reson. Chem.* **1987**, *25*, 60. (f) Hirota, N.; Weissman, S. I. *J. Am. Chem. Soc.* **1964**, *86*, 2538. (g) Grampp, G.; Landgraf, S.; Rasmussen, K.; Strauss, S. *Spectrochim. Acta A* **2002**, *58*, 1219. (h) Zheng, S.; Lan, J.; Khan, S. I.; Rubin, Y. *J. Am. Chem. Soc.* **2003**, *125*, 5786. (i) Gerson, F. *Helv. Chim. Acta* **1966**, *49*, 1463. (j) Bowman, D. F.; Gillan, T.; Ingold, K. U. **1971**, *93*, 6555. (k) Mendenhall, G. D.; Ingold, K. U. *J. Am. Chem. Soc.* **1972**, *94*, 7166.
(16) Ganesan, V.; Rosokha, S. V.; Kochi, J. K *J. Am. Chem. Soc.* **2003**, *125*, 2559.

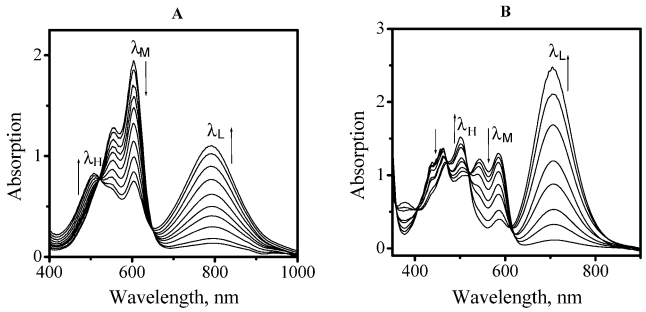

Figure 1. Temperature modulated spectral changes in dichloromethane solution of cation and anion radicals ($l = 0.1$ cm). (A) $\mathbf{OMB}^{+\bullet}SbCl_6^-$ ($c_0 = 1.5$ mM), temperature (°C): −43, −55, −65, −70, −73, −78, −84, −86, −90, −92 (bottom to top at 800 nm). (B) $\mathbf{DDQ}^{-\bullet}Bu_4N^+$ ($c_0 = 2.0$ mM), temperature (°C): −44, −57, −66, −75, −81, −89, −97, −102 (bottom to top at 750 nm).

prepared as the crystalline hexachloroantimonate salt, was indicated by the temperature and concentration-dependent spectrum consisting of three groups of diagnostic absorption bands with maxima labeled λ_M, λ_L, and λ_H in Figure 1A. At constant temperature, the intensities of the twin absorptions λ_L and λ_H were proportional to the square of the concentration of [$\mathbf{OMB}^{+\bullet}SbCl_6^-$] in dichloromethane (see Figure S1B in the Supporting Information). With increasing dilutions of the $\mathbf{OMB}^{+\bullet}$ solution, bands λ_H/λ_L gradually diminished and finally disappeared, until only the unchanging spectrum $\lambda_M = 602$ nm with a minor satellite at 555 nm remained at high dilutions of ~0.1 mM. The intensity of λ_M was linearly related to the initial salt concentration and was essentially temperature independent at the concentration of [$\mathbf{OMB}^{+\bullet}SbCl_6^-$]$_0$ < 0.1 mM. By contrast, Figure 1A shows that the prominent near-IR band $\lambda_L = 792$ nm, as well as λ_H, increased substantially when the temperature of a 1.5 mM solution of the biphenylene cation radical was progressively lowered. The clear existence of a pair of well-defined isosbestic points in Figure 1A established the quantitative interchange between the two species characterized by λ_M and λ_H/λ_L. The linear dependence of the absorbance of the λ_M band and the quadratic dependence of λ_H/λ_L bands with concentration allowed us to assign λ_M to the monomeric species ($\mathbf{OMB}^{+\bullet}$) and λ_L/λ_H to the dimeric form $(\mathbf{OMB})_2^{2+}$, the extinction coefficients of which are included in Table 1; see Experimental Section for details.

(17) (a) Lewis, L. C.; Singer, L. S. *Chem. Phys.* **1965**, *43*, 2712. (b) Howarth, O. W.; Fraenkel, G. K. *J. Am. Chem. Soc.* **1966**, *88*, 4514. (c) Howarth, O. W.; Fraenkel, G. K. *J. Chem. Phys.* **1970**, *52*, 6258. (d) Badger, B.; Brocklehurst, B. *Nature* **1968**, *219*, 263. (e) Badger, B.; Brocklehurst, B.; Dudley, R. *Chem. Phys. Lett.* **1967**, *1*, 122. (f) Badger, B.; Brocklehurst, B. *Trans. Faraday Soc.* **1969**, *65*, 2582. (g) Badger, B.; Brocklehurst, B. *Trans. Faraday Soc.* **1969**, *65*, 2588. (h) Badger, B.; Brocklehurst, B. *Trans. Faraday Soc.* **1970**, *66*, 2939. (i) Meot-Ner, M.; Hamlet, P.; Hunter, E. P.; Field, F. H. *J. Am. Chem. Soc.* **1978**, *100*, 5466. (j) Meot-Ner, M. *J. Phys. Chem.* **1980**, *84*, 2724. (k) Meot-Ner, M.; El-Shall, M. S. *J. Am. Chem. Soc.* **1986**, *108*, 4386. For the spectral and structural characterization of such cation-radical "pimers", see: (l) Le Magueres, P.; Lindeman, S.; Kochi, J. K. *J. Chem. Soc., Perkin Trans 2* **2001**, 1180. (m) Kochi, J. K.; Rathore, R.; Le Magueres, P. in ref 12a and references therein. (n) Extensive electron delocalizations in the π-bonded pimers are indicated in the EPR spectra by twice the number of hyperfine lines with half the splittings observed in the monomeric radical. (o) Note that $(\mathbf{OMB})_2^{+\bullet}$ is a three-electron pimer[12] as opposed to $(\mathbf{TCNE})_2^{-\bullet}$ or $(\mathbf{PHEN})_2^{+\bullet}$ which are one-electron pimers. (p) Compare also Dewar's putative structure pertinent to the benzidene and related rearrangement. See, e.g., Miller, B. *Advanced Organic Chemistry*, 2nd ed.; Pearson/Prentice Hall, New York, 2003; p 119.

(18) (a) Goldstein, P.; Seff, K.; Trueblood, K. N. *Acta Crystallogr.* **1968**, *B24*, 778. (b) Hanson, A. W. *Acta Crystallogr.* **1968**, *B24*, 773. (c) Kobayashi, H. *Bull. Chem. Soc. Jpn.* **1974**, *47*,1346. (c) Fourmigue, M.; Perrocheau, V.; Clerac, R.; Coulon, C. *J. Mater. Chem.* **1997**, *7*, 2235. (d) Ballester, L.; Gutierrez, A.; Perpinan, M. F.; Rico, S.; Azcondo, M. T.; Bellito, C. *Inorg. Chem.* **1999**, *38*, 4430.

Table 1. Spectral Characteristics of Cationic, Neutral, and Anionic Radicals and Their Dimers[a]

parent donor or acceptor[b]	π-radical	monomeric species[c]	dimeric species		
		λ_M (log ϵ_M)	λ_H (log ϵ_H)	λ_L (log ϵ_L)	$h\nu_L$
OMB	$\mathbf{OMB}^{+\bullet}SbCl_6^-$	602 (4.1) (blue)	505 (4.2)	792 (4.4) (purple)	1.57
PHEN$^+$	**PHEN**$^\bullet$	544 (2.0) (pink)	*d*	595 (4.3) (blue)	2.09
DDQ	$Bu_4N^+\mathbf{DDQ}^{-\bullet}$	588 (3.8) (maroon)	502 (4.3)	710 (4.5) (green)	1.75
TCNQ	$Bu_4N^+\mathbf{TCNQ}^{-\bullet}$	845 (4.6) (green)	643 (4.5)[e]	870 (4.1)[e] (cyan)	1.43
TCNE	$Bu_4N^+\mathbf{TCNE}^{-\bullet}$	428 (3.9) (yellow)	*f* 370 (4.0)[g]	525 (4.3) 530(4.2)[g] (red)	2.36 2.34
CA	$Bu_4N^+\mathbf{CA}^{-\bullet}$	450 (4.0) (yellow-red)	*f* 380 (4.0)[h]	680 (4.2) 670(4.1)[h] (green)	1.82 1.85

[a] In dichloromethane solutions, unless otherwise noted; in the visible−NIR spectral range (350−1000 nm). Wavelength of band maxima λ (in nm); in parentheses, the logarithm of extinction coefficients ϵ; the transition energy $h\nu_L$ in eV. [b] As determined in Charts 2 and 3. [c] Principal band in visible−NIR range for monomeric species. For other absorption bands of a monomeric radical, wavelengths (in nm) and logarithm of extinction coefficients (in parentheses) are the following: $\mathbf{OMB}^{+\bullet}$, 555 (3.9); $\mathbf{PHEN}^\bullet$, 374 (3.5), 393(2.5); $\mathbf{DDQ}^{-\bullet}$, 460(3.8), 547(3.7); $\mathbf{CA}^{-\bullet}$, 424 (3.8); $\mathbf{TCNQ}^{-\bullet}$, 422 (4.4), 745(4.3), 763(4.3), 824(4.4). Absorption band of $\mathbf{TCNE}^{-\bullet}$ vibronically split with maxima at 400, 410, 420, 428, 438, 447, 457, and 467 nm. [d] λ_H not observed (related intramolecular transition in the monomer is very weak). V. Zaitsev, unpublished results. [e] In H_2O, ref 14b. In dichloromethane, the dimers bands obscured by intense bands of monomer at all accessible temperature/concentrations. [f] In dichloromethane, λ_H band obscured by the monomer absorption at all accessible temperatures/concentrations. [g] In MTHF (from $Na^+\mathbf{TCNE}^{-\bullet}$), ref 14c. [h] In EtOH, (from $Na^+\mathbf{CA}^{-\bullet}$), ref 15k.

The same combination of concentration adjustment and temperature modulation was used to segregate the monomeric and dimeric species of the neutral radical $\mathbf{PHEN}^\bullet$ and of the anion radicals of the π-acceptors in Chart 2, as shown by the typical spectral changes of the anion-radical $\mathbf{DDQ}^{-\bullet}$ in Figure 1B (see Experimental Section and Figures S2−S4 in the Supporting Information for details). The spectral characteristics of each monomeric and dimeric species including their characteristic colors in dichloromethane solution are summarized in Table 1.

B. Energetics of Monomer/Dimer Interconversion via UV−Vis Measurements in Solution. The temperature-dependent spectral changes were highly reproducible and pointed to the reversible equilibrium in eq 1,

$$\mathbf{OMB}^{+\bullet} + \mathbf{OMB}^{+\bullet} \overset{K_D}{\rightleftharpoons} (\mathbf{OMB})_2^{2+} \qquad (1)$$

which was quantitatively evaluated for the concentrations of both monomeric and dimeric forms based on the extinction coefficients in Table 1, columns 3 and 5. The fraction of monomer α_M was found to be highly dependent on temperature as well as the initial concentration of $\mathbf{OMB}^{+\bullet}SbCl_6^-$ as shown in Figure 2.Thus, α_M was evaluated at different concentrations and temperatures according to eq 1 and yielded the equilibrium constants K_D in Table 2, column 2 and Table S1.

The enthalpy and entropy for dimer formation were obtained from the linear temperature dependence shown in the Figure 2 inset; the values of ΔH_D and ΔS_D are listed in Table 2 (columns 3 and 4).

The *calculated* concentration dependence of the monomeric and dimeric species with temperature were based on the

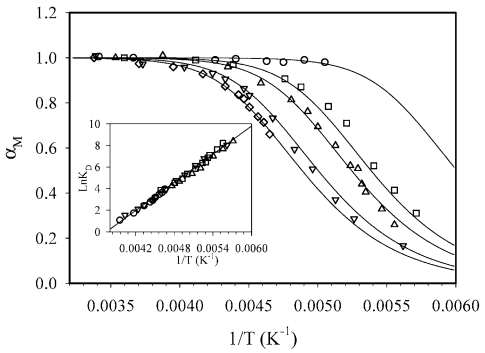

Figure 2. Temperature dependence of the monomer fraction α_M in dichloromethane solution of **OMB**$^{+\bullet}$$SbCl_6^-$ at initial concentrations: 0.1 mM (○), 0.8 mM (□), 1.5 mM (△), 4.9 mM (▽), 7.4 mM (◇). Solid lines: calculated dependence based on $\Delta H = -8.8$ kcal/mol and $\Delta S = -33$ eu. Inset: temperature dependence of the dimerization constant K_D.

Table 2. Energetics of π-Dimerization in Solution by UV−vis and EPR Spectral Measurements

	UV−vis measurements			EPR measurements		
radical[a]	K_D[b] (M^{-1})	$-\Delta H_D$[c] (kcal mol^{-1})	$-\Delta S_D$[d] (eu)	K_D[b] (M^{-1})	$-\Delta H_D$[c] (kcal mol^{-1})	$-\Delta S_D$[d] (eu)
OMB$^{+\bullet}$	0.22 ± 0.05	9.0	33	0.23 ± 0.05	8.8	32
PHEN$^{\bullet}$[h]	0.16 ± 0.08	8.8	33	0.15 ± 0.08	9.5	36
DDQ$^{-\bullet}$	0.28 ± 0.05	7.6	28	0.27 ± 0.05	9.0	33
TCNQ$^{-\bullet}$	*f*	*e*	*e*	$\sim 5 \times 10^{-3}$	9.8	42
TCNE$^{-\bullet}$	$\sim 7 \times 10^{-4}$	8.8	41	$\sim 10^{-3}$ *f*	7.9*f*	36*f*
CA$^{-\bullet}$	$\sim 1 \times 10^{-3}$	6.0	33	*g*	*g*	*g*

[a] As in Table 1. [b] In dichloromethane at 298 K. [c] ±1 kcal mol^{-1}. [d] ±3 eu. [e] Dimer bands overlapped by the strong monomer absorption. [f] Estimates owing to apparent spectral hysteresis of the temperature modulation. [g] Measurements unreliable at the very low temperature required. [h] V. Zaitsev, unpublished results.

thermodynamic parameters in Table 2, and these are shown as solid lines in Figure 2. Most importantly, the unmistakable fits of the curved lines to the families of experimental data (dots) further confirm the assignment of the spectral changes to the monomer/dimer equilibrium according to eq 1.

The same spectral analysis of the concentration and temperature dependence was applied to the spectral changes of the neutral phenalene radical **PHEN**$^{\bullet}$ and to the π-dimerization of the anion radicals of π-acceptors; for example,

$$\mathbf{TCNE}^{-\bullet} + \mathbf{TCNE}^{-\bullet} \overset{K_D}{\rightleftharpoons} [\mathbf{TCNE},\mathbf{TCNE}]^{2-} \qquad (2)$$

see Supporting Information for details; the pertinent thermodynamic data are included in Table 2.

C. EPR Spectral Changes of Radical Dimerization in Solution. EPR spectra of the neutral, cationic, and anionic radicals derived from the precursors in Charts 2 and 3 were all rigorously characterized in dichloromethane solution by their well-resolved hyperfine splittings. For example, the spectrum of **PHEN**$^{\bullet}$ consisted of the binomial septet for six equivalent protons with $a_{6H} = 6.2$ G, $g = 2.0028$.[11] Analogously, the cation radical of the aromatic hydrocarbon **OMB** (Chart 3) consisted of the binomial tridecet for the 12 equivalent protons of 4 perimethyl groups with $a_{12H} = 4.5$ G.[12a] Furthermore, the EPR spectra of the anion radicals of the acceptors in Chart 2 accorded with the literature citations, as confirmed by the results described in Figures S5 and S6 of the Supporting Information.

Although the line widths of the EPR spectra remained singularly invariant upon cooling the dichloromethane solutions

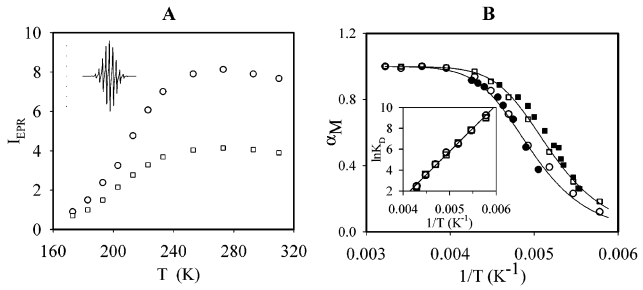

Figure 3. Temperature dependence of (A) the EPR intensity (I_{EPR}) and (B) the monomer fraction α_M of the cation-radical **OMB**$^{+\bullet}$ with $c_0 = 1.5$ mM (squares) and 3 mM (circles) in CH_2Cl_2 (the open symbols are from EPR measurements, and the filled symbols, from UV−vis measurements). Solid lines: the calculated dependence based on the same concentrations with a ΔH of −8.8 kcal/mol and ΔS of −32 eu. Insets: (A) EPR spectrum of **OMB**$^{+\bullet}$, (B) temperature dependence of the dimerization constant K_D.

of all radicals independent of their charge, the substantial variations of their intensity were unmistakable. The typical profile obtained by double integration of the EPR spectrum of **OMB**$^{+\bullet}$ is shown in Figure 3A. The gradual increase of the intensity of the EPR signal of **OMB**$^{+\bullet}$ accords with its expected Curie−Weiss behavior together with other extraneous factors described in the Experimental. However, the further lowering of the temperature resulted in the precipitous diminution of the signal intensity indicative of a sharp drop in the concentration of the monomeric species **OMB**$^{+\bullet}$. Indeed, the quantitative analysis of the EPR intensity coupled to appropriate controls allowed the Curie−Weiss effects and the extraneous factors to be separated from the consequences of changing radical concentrations; see Experimental Section for details. Since such temperature-dependent intensity changes were quite reversible, and the deviation from the Curie−Weiss behavior was more pronounced with increasing initial concentrations of the radical, the major drop in signal intensity was assigned to the formation of diamagnetic EPR-silent dimers according to eq 1. As a result, the dimerization constant could be readily obtained from the fraction of the monomeric radical (**OMB**$^{+\bullet}$) evaluated directly from the EPR spectral data. The linear temperature dependence of ln K_D shown in the Figure 3B inset afforded the thermodynamic parameters in Table 2.

Most importantly, the temperature dependence of the monomer fraction in Figure 3B, as determined by EPR measurements of **OMB**$^{+\bullet}$ coincided with that derived from the UV−vis studies at the same concentrations. Similar agreement was observed for the neutral radical **PHEN**$^{\bullet}$ and the anion radicals from Chart 2, see Supporting Information. The values of K_D, as well as thermodynamic parameters ΔH_D and ΔS_D, in Table 2 demonstrate that (1) both spectral (EPR, UV−vis) changes accurately and quantitatively reflect the temperature/concentration modulation of the reversible radical/radical dimerization and (ii) the radical dimers are consistently diamagnetic and characterized by distinctive electronic transitions which are substantially different from those of the monomeric parents.

D. Effect of the Cationic Counterion in Solution. Since ion-pairing energies are maximized in media of lowest polarity, we chose acetone as an optimum solvent for the study of the electrostatic effect of various cationic counterions on anion radicals owing to (a) its moderate dielectric constant and reasonable inertness to radicals, (b) its ability to dissolve anion-radical salts of different counterions, and (c) its extended range

Table 3. Counterion Effects on the Spectral Characteristics of $DDQ^{-\bullet}$ Monomer (M) and Dimer (D) and the Thermodynamics of Its Dimerization (in Acetone)

counterion	λ_M (nm)	ϵ_M (10^3 M^{-1} cm^{-1})	λ_D (nm)	ϵ_D (10^3 M^{-1} cm^{-1})	$-\Delta H_D$[a] (kcal/mol)	$-\Delta S_D$[b] (eu)	K_D[c] (M^{-1})
Na^+	595	6.3	700	32	7.1	31	0.03 ± 0.01
K^+	595	6.3	700	31	8.1	35	0.022 ± 0.007
Me_4N^+	595	6.3	700	35	8.2	37	0.025 ± 0.007
Et_4N^+	595	6.3	700	33	8.1	34	0.027 ± 0.005
Pr_4N^+	595	6.3	700	33	8.3	36	0.020 ± 0.007
Bu_4N^+	600	6.0	700	35	8.3	36	0.020 ± 0.007

[a] ± 1 kcal mol^{-1}. [b] ± 3 eu. [c] At 298 K.

Table 4. Solvent Effects on the Spectral Characteristics of Bu_4N^+**DDQ**$^{-\bullet}$ Monomer (M) and Dimer (D) and the Thermodynamics of Its Dimerization

solvent	λ_M (nm)	ϵ_M (10^3 M^{-1} cm^{-1})	λ_D (nm)	ϵ_D (10^3 M^{-1} cm^{-1})	$-\Delta H_D$[a] (kcal/mol)	$-\Delta S_D$[b] (eu)	K_D[c] (M^{-1})
CH_2Cl_2	585	6.3	710	33	7.6	28	0.28 ± 0.05
$(CH_3)_2CO$	600	6.3	700	35	8.3	36	0.020 ± 0.007
EtCN	595	6.3	700	35	9.5	37	0.08 ± 0.01
PrCN	595	6.3	700	35	9.5	40	0.029 ± 0.010

[a] ± 1 kcal mol^{-1}. [b] ± 3 eu. [c] At 298 K.

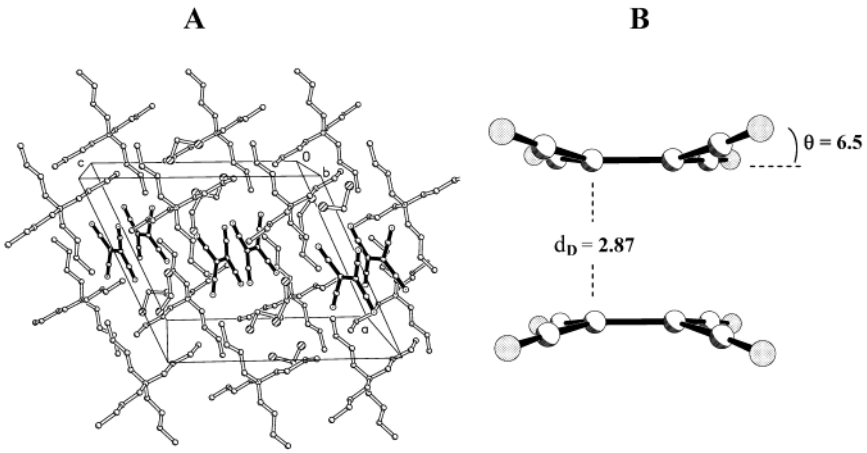

Figure 4. (A) Crystal structure representation of unit cell of **TCNE**$^{-\bullet}$$(Bu_4N)^+$ showing the packing of discrete pairs of anion radicals. (B) Side perspective view of the dimeric pair of **TCNE**$^{-\bullet}$ anion radicals showing their concave shape with $\theta = 6.5°$.

for temperature variation. The results in Table 3 necessarily focused on **DDQ**$^{-\bullet}$ because the same series of **TCNE**$^{-\bullet}$ salts were rather insoluble in this medium.[19a] The spectral properties of both the monomeric as well as the dimeric forms of **DDQ**$^{-\bullet}$ and the thermodynamic parameters for dimerization were unaffected by the change in either the size or the nature of the countercation.[19b]

E. Effect of Solvent on π-Dimerization. Although medium effects on various equilibria are difficult to interpret quantitatively, the results of the π-dimerizations of anion radicals show some striking and informative characteristics in different solvents. A few representative variations of the spectral and thermodynamic properties on the π-dimerization of **DDQ**$^{-\bullet}$ are presented in Table 4, and a more extensive compilation taken from the literature is presented in Table S2 of the Supporting Information. The scrutiny of all the data in toto reveals a single inescapable observation of solvent effects on the π-dimerization of **DDQ**$^{-\bullet}$; namely, the spectral properties (λ, ϵ) of both the monomeric and dimeric forms are singularly unaffected under conditions in which the thermodynamic properties (K_D, ΔH_D, ΔS_D) vary widely in different solvents.

II. X-ray Crystallography of π-Bonded Dimers. A. From Tetracyanoethylene Anion Radical. Slow diffusion of hexane into a dilute solution of **TCNE**$^{-\bullet}$ as the tetra-*n*-butylammonium salt in dichloromethane at -70 °C resulted in the formation of highly unstable dark brown crystals with the overall composition [Bu_4N^+**TCNE**$^{-\bullet}$, $2CH_2Cl_2$]; the significant presence of solvent in the unit cell necessitated their careful handling at low temperatures. X-ray crystallographic analysis at $-150°$ C revealed the existence of a series of discrete dimeric units derived from two **TCNE**$^{-\bullet}$ (Figure 4A) and separated by a pair of C−C bonds with $d_D = 2.87$ Å (Figure 4B).[20] The long distances of ~10 Å between such $(\mathbf{TCNE})_2^{2-}$ units provide unequivocal evidence of the formation of discrete dimers in the

(19) (a) For the counterion effect in methyltetrahydrofuran, see Itoh in ref 14c. (b) Since solubility limitations of these crystalline salts precluded the use of organic solvents of low polarity, we were unable to provide a more stringent test of the counterion effects (especially tetraalkylammonium versus alkali metal) on ion-pairing equilibria beyond that provided by acetone of moderate polarity. Nonetheless, the extensive solvent effects in Table 4 are sufficient to establish the important point that generalized ion-pairing effects do not materially affect the spectral properties of the dimer (columns 4 and 5) to the large degree that they affect the thermodynamic parameters (columns 6, 7, and 8).

(20) (a) X-ray crystallography of the corresponding tetra-*n*-propylammonium salt by Miller and co-workers[b] revealed the presence of the same dimeric units in the unit cell with $d_D = 2.87$ Å. (b) Del Sesto, R. E.; Botoshansky, M.; Kaftory, M.; Miller, J. S. *Cryst. Eng. Comm.* **2002**, *4*, 106.

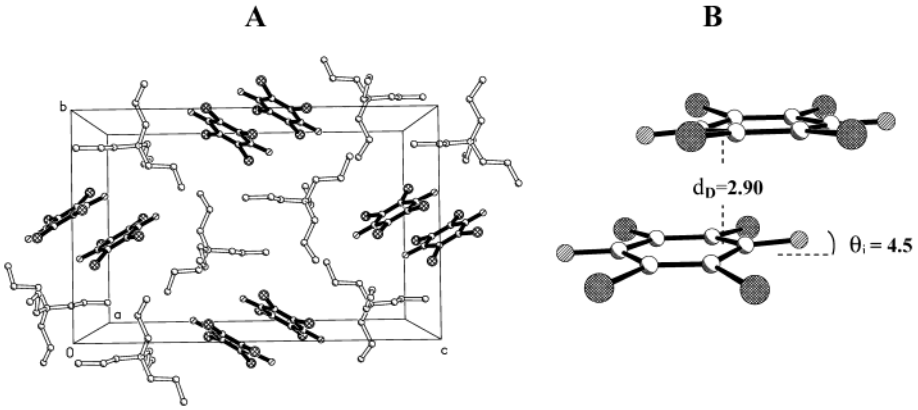

Figure 5. (A) Crystal structure representation of the unit cell of $\mathbf{CA}^{-\bullet}(Pr_4N)^+$ showing the packing of discrete pairs of anion radicals. (B) Side perspective view of the pair of $\mathbf{CA}^{-\bullet}$ anion radicals with $\theta_i = 4.5°$ and $\theta_o = 0°$.

crystalline solid state. With one exception, the bonding parameters[21] in each **TCNE** moiety of the dimeric unit are essentially those of the monomeric form of $\mathbf{TCNE}^{-\bullet}$, which could be independently analyzed as yellow crystals obtained via direct crystallization of the monomeric salt $Bu_4N^+\mathbf{TCNE}^{-\bullet}$ from acetonitrile.[22] The lone exception in the structural parameters of the centrosymmetric dimeric unit is the detectable bending of the two pairs of geminal cyano groups out of the C−C plane by the dihedral angle $\theta = 6.5°$ (see Figure 4B). Importantly, the four bulky butyl "arms" prevent close contacts with the counterions, the closest distance between the nitrogen centers on tetracyanoethylene and tetrabutylammonium being 4.4 Å. As a result, the attractive cation/anion electrostatic forces pose minimal detraction from the pertinent radical/radical interaction within the dimeric unit.

B. From Chloranil Anion Radical. X-ray crystallographic analyses of chloranil anion-radical crystals followed essentially the same pattern as those observed for the tetracyanoethylene analogues. Thus, the slow diffusion of the *n*-hexane into a dilute solution of the chloranil anion radical as the tetra-*n*-propylammonium salt in dichloromethane at −70 °C yielded rhombic brown crystals with the overall composition $[Pr_4N^+\mathbf{CA}^{-\bullet}]$. The X-ray crystallographic analysis at −150 °C revealed the presence of a series of discrete dimeric units derived from two $\mathbf{CA}^{-\bullet}$ (Figure 5A), in which the coplanar but the characteristically "slipped" **CA** moieties are separated by an interplanar distance of $d_D = 2.9$ Å (Figure 5B). The bonding parameters within each **CA** moiety[23] of the dimeric unit are essentially those of the monomeric form of $\mathbf{CA}^{-\bullet}$ which could be independently analyzed as the monosolvate $[Pr_4N^+\mathbf{CA}^{-\bullet}, CH_2Cl_2]$.[16] However, each centrosymmetric dimeric unit suffers a unique distortion from planarity in which only the inner carbonyl dipoles lying directly below (or above) are bent by $\theta_i = 4.5°$ toward the upper (or lower) **CA** moiety. The pair of outer carbonyl groups with $\theta_o = 0°$ maintain their coplanarity with the planar six-membered ring. These chloranil dimers are well separated within the crystal, with distances between dimeric units of ∼10 Å.

C. From Other π-Radicals. Crystallographic data for $\mathbf{TCNQ}^{-\bullet}$ and $\mathbf{DDQ}^{-\bullet}$ anion radicals with different counterions are widely available in the literature. Although many crystal structures involve homosoric stacks of anion-radical units,[27] there are clear indications of intermolecular radical/radical associations.[2,3] Typical interplanar distances in such dimeric associates are $d_D \approx 3.2$ Å for $\mathbf{TCNQ}^{-\bullet}$ and $d_D \approx 2.9$ Å for $\mathbf{DDQ}^{-\bullet}$.[2,10] Solid-state electron-spectroscopic studies indicate the presence of new low-energy absorption bands, akin to those observed for the corresponding dimers in solutions.[6,14c,24] The crystal structure of $\mathbf{PHEN}^{\bullet}$ shows the formation of dimeric pairs with interplanar separations of about $d_D \approx 3.22$ Å and a staggered arrangement of the *tert*-butyl groups to minimize steric repulsions.[11] The electronic spectrum of these crystals consists of a broad absorption band in the UV−vis region around 600 nm which is similar to the spectrum of the dimer $(\mathbf{PHEN})_2$ in dichloromethane solution. The analysis of crystal structure of the octamethylbiphenylene salt $\mathbf{OMB}^{+\bullet}SbCl_6^-$ shows that it is packed as pairs of cation radicals with interplanar separations of $d_D = 3.05$ Å which are isolated by pairs of anions in infinite alternating stacks.[12] The close cofacial proximity of two identical $\mathbf{OMB}^{+\bullet}$ moieties induces a slight bending of the biphenylene ring system with a dihedral angle of 6.3° between the mean planes of the benzene rings. The solid-state spectrum of the

(21) The bonding parameters in the dimeric unit $(\mathbf{TCNE})_2^{2-}$ are C−C 1.428 Å, C−CN 1.422 Å, and C≡N 1.145 Å, and NC−C−CN 118.4° with θ = 6.5°; the corresponding parameters in monomeric $\mathbf{TCNE}^{-\bullet}$ are 1.429, 1.405, and 1.170 Å and 117.7° with $\theta = 0°$.[22b]

(22) (a) The cell parameters of these crystals were identical with those previously obtained by Miller and co-workers[22b] of the monomeric structures of $\mathbf{TCNE}^{-\bullet}$. (b) Zheludev, A.; Grand, A.; Ressouche, E.; Schwiizer, J.; Morin, B. G.; Epstein, A. J.; Dixon, D. A.; Miller, J. S. *J. Am. Chem. Soc.* **1994**, *116*, 7243.

(23) The bonding parameters in the dimeric unit $(\mathbf{CA})_2^{2-}$ are (Cl)C−C(Cl) 1.364 Å, (Cl)C−C(O) 1.454 Å, C−O 1.251 Å, and C−Cl 1.726 Å.

(24) (a) Iida, Y. *Bull. Chem. Soc. Jpn.* **1969**, *42*, 637. (b) Oohashi, Y.; Sakata, T. *Bull. Chem. Soc. Jpn.* **1973**, *46*, 3330.

(25) For example, see: (a) Hove, M. J.; Hoffman B. M.; Ibers, J. A. *J. Chem. Phys.* **1971**, *56*, 3490. (b) Guirauden, A.; Johannsen, I.; Batail, P.; Coulon, C. *Inorg. Chem.* **1993**, *32*, 2446. (c) Yakushi, K.; Nishimura, S.; Sugano, T.; Kuroda, H. *Acta Crystallogr.* **1980**, *B36*, 358. (d) Attanasio, D.; Bellitto, C.; Bonamico, M.; Fares, V.; Imperatori, P. *Gazz. Chim. Ital.* **1991**, *121*, 155. (e) Forward, J. M.; Mingos, D. M. P.; Muller, T. E.; Williams, D. J.; Yan, Y.-K. *J. Organomet. Chem.* **1994**, *467*, 207.

(26) (a) Sebastiano, R.; Korp, J. D.; Kochi, J. K. *J. Chem. Soc. Chem. Commun.* **1991**, 1481. (b) Bockman, T. M.; Kochi, J. K. *J. Org. Chem.* **1990**, *55*, 4127. (c) Hilgers, F.; Kaim, W.; Schulz, A.; Zalis, S. *J. Chem. Soc., Perkin Trans 2* **1994**, 135. (d) Song, H.; Reed, C. A.; Scheidt, W. R. *J. Am. Chem. Soc.* **1989**, 111, 6867. (e) Nagashima, H.; Hashimoto, N.; Inoue, H.; Yoshioka, N. *New J. Chem.* **2003**, *27*, 805.

(27) (a) In charge-transfer crystals, packing of the donor (D) and acceptor (A) units can occur in either two separate DDD and AAA stacks (homosoric) or single alternating DADA stacks (heterosoric). (b) Planar π-radicals most commonly appear in crystals as homosoric stacks (vertical and oblique) in which the interplanar separation d_D is not strongly different from that *between* dimer units. The counterion is most often located by the sides of the stack. By contrast, only those crystals containing *discrete* dimeric units and separated from neighboring dimers by intervening counterions are included in Table 5. (c) For the recent classification of radical compounds according to crystal structure, see: Dahm, D. J.; Horn, P.; Johnson, G. R.; Miles, M. G.; Wilson, J. D. *J. Cryst. Mol. Struct.* **1975**, *5*, 27.

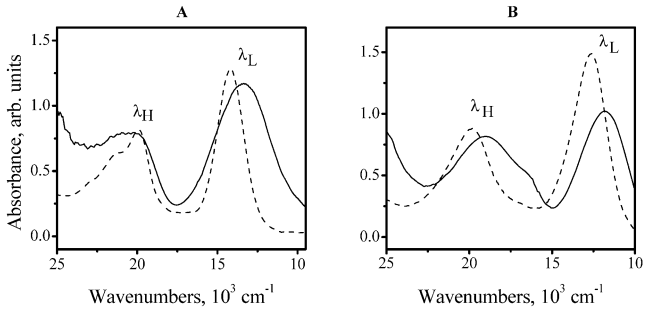

Figure 6. Electronic spectra of the dimeric radical salts of (A) **DDQ**$^{-\bullet}$ Pr_4N^+ and (B) **OMB**$^{+\bullet}SbCl_6^-$ in the solid state (KBr, solid line) and in dichloromethane solution (dashed line derived from the temperature dependence in Figure 1; see Supporting Information for details).

Table 5. Spectral Comparison of the Charge-Transfer Transitions of (Radical/Radical) Dimers in Dichloromethane Solution and in the Solid State (KBr)

	solution		solid state	
radical	λ_H (nm)	λ_L (nm)	λ_H (nm)	λ_L (nm)
Pr_4N^+**TCNE**$^{-\bullet}$	370[a]	525	380[b]	546[b]
Pr_4N^+**DDQ**$^{-\bullet}$	502	710	490	750
OMB$^{+\bullet}SbCl_6$	505	792	525	845
PHEN$^{\bullet}$	*c*	595[d]	*c*	612[e]

[a] In MTHF; see Table 1. [b] Reference 5. [c] The high-energy band not observed; see Table 1. [d] V. Zaitsev, unpublished results. [e] Reference 11a.

crystals contains a broad absorption band in the NIR region around 800 nm (Figure 6) akin to that of the dimeric form $(\mathbf{OMB})_2^{2+}$ in dichloromethane solution. Finally, there are a number of references in the solid-state literature of crystalline dimeric units for other stable π-radicals such as those derived from fulvalenes and *p*-phenylenediamine derivatives, methyl viologen, octamethylanthracene, and so forth.[25,26]

III. Comparative Spectral Studies of the π-Dimers in Solution and in the State Solid. Electronic spectra of the dimeric forms of the neutral radical (**PHEN**$^{\bullet}$), the cation radical (**OMB**$^{+\bullet}$), and the anion radicals (**TCNE**$^{-\bullet}$, **TCNQ**$^{-\bullet}$, **DDQ**$^{-\bullet}$, **CA**$^{-\bullet}$) in solution are all characterized by rather intense, distinctive absorptions λ_L in the far UV/near-IR regions, as listed in Table 1, column 5. Typical absorption spectra of solid-state samples in Figure 6, obtained as either dilute suspensions in mineral oil (Nujol) or KBr mull, also showed these diagnostic NIR bands with λ_L slightly red-shifted relative to those in solution.[5,14c,24] Moreover, the second high-energy band λ_H appeared in the solid-state spectra with more or less the same absorbance ratio relative to λ_L as that observed in solution.[14c,24] The minor but consistent red-shifts of both λ_L and λ_H in the solid-state spectra are presented in Table 5 for all those crystalline samples in which X-ray crystallography has independently established the presence of discrete dimeric units.[27]

Discussion

Combined spectroscopic UV−vis−NIR and EPR studies in solution establish the reversible dimerization of the π-radicals derived from the precursors depicted in Charts 2 and 3. Facility and spontaneity at low temperatures are the characteristics of all the quantitative dimerizations, irrespective of the resident electrical charge (+, 0, −) on the paramagnetic species. Most importantly, the resultant π-bonded diamagnetic dimers, both doubly charged as well as uncharged, strongly share three striking facets in common, namely: (I) diagnostic electronic

Chart 4

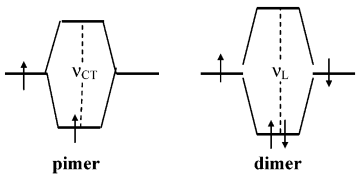

transitions in the near-IR, (II) unusual energetics (ΔH_D, ΔS_D) of formation, and (III) diamagnetic dimeric structures with long-bonded interactions, as elaborated in following.

I. Electronic Transition in the π-Bonded Dimer. The outstanding and unique spectral feature of all the π-bonded dimers is the presence of broad absorptions in the near-IR region with large transition moments listed as λ_L (log ϵ_L) in Table 1, last column and typically illustrated as the lowest-energy bands in Figure 1. Indeed, such spectral characteristics are highly reminiscent of those we recently identified in the paramagnetic pimers that result from the reversible π-association of the corresponding free radical with its diamagnetic counterpart; for example,[16]

$$\mathbf{TCNE}^{-\bullet} + \mathbf{TCNE} \overset{K_p}{\rightleftharpoons} [\mathbf{TCNE},\mathbf{TCNE}]^{-\bullet} \qquad (3)$$

Strictly speaking, the intermolecular interaction of the tetracyanoethylene anion radical (K_P) leading to the pimer in eq 3 is tantamount to its self-association leading to dimer formation (K_D) in eq 2 because these twin processes differ by the presence or absence of only a single electron. Thus, the charge-transfer description of the electronic transition that was previously described successfully for the paramagnetic pimers in Chart 4 (left)[16] can also be directly applied to the corresponding diamagnetic π-dimers, as shown in Chart 4 (right).

According to the basic LCAO molecular-orbital description in Chart 4 (left), the paramagnetic pimer $(\mathbf{TCNE})_2^{-\bullet}$ derives from the frontier-orbital interaction of the open-shell SOMO and the closed-shell LUMO of tetracyanoethylene. Likewise, the diamagnetic dimer $(\mathbf{TCNE})_2^{2-}$ derives from an analogous frontier-orbital interaction of a pair of equivalent SOMOs shown in Chart 4 (right). In both cases, the orbital mixings are akin to those encountered in charge-transfer formulations based on Mulliken theory.[28] Accordingly, the diagnostic NIR bands in Table 1 correspond to the electronic transition from the bonding to antibonding orbital, the transition energy of which can be evaluated as[29] $h\nu_L = (\Delta^2 + 4H_{ab}^2)^{1/2}$, where Δ is the energy difference between the interacting orbitals (ψ_b and ψ_a) and the electronic-coupling element H_{ab} is equated to the resonance

(28) (a) Mulliken, R. S. *J. Am. Chem. Soc.* **1952**, *74*, 811. (b) Mulliken, R. S. *J. Phys. Chem.* **1952**, *56*, 801. For the equivalent molecular-orbital formulation, see: (c) Flurry, R. L. *J. Phys. Chem.* **1965**, *69*, 1927. (d) Flurry, R. L. *J. Phys. Chem.* **1969**, *73*, 2111. (e) Flurry, R. L. *J. Phys. Chem.* **1969**, *73*, 2787. (f) Since the charge-transfer formulation has generally been applied to wholly diamagnetic systems,[30d−f] dimer formation as in eqs 1 and 2 can be alternatively considered from an equivalent point of view that starts from a pair of closed-shell species such as a dication and its neutral donor or a dianion and its neutral acceptor, which are more traditional charge-transfer dyads. Indeed, such an analogy has been realized in the methyl viologen systems.[26b]

(29) The derivation of the $h\nu_L$ relationship is based on neglect of direct overlap of the π-orbitals, and we thus intend its use here to be only qualitative in nature. A more quantitative treatment of this subject will be presented in a forthcoming paper (Sun, D. L.; Rosokha, S. V.; Lindeman, S. V.; Kochi, J. K. Submitted for publication).

integral $\int \psi_b H^{eff} \psi_a$.[29−31] Since Δ is nil in π-dimerization, the transition energy $h\nu_L$ in π-bonded dimers is directly related to the electronic-coupling term H_{ab}. We conclude from the rather narrow span of ±0.35 eV[32] in the transition energies ($h\nu_L$ in Table 1) that the electronic coupling elements are also rather invariant in the series of π-bonded dimers, independent of whether they are doubly charged or neutral since the weakest electronic coupling is observed in the dicationic dimer $(\mathbf{OMB})_2^{2+}$, the strongest is observed in the dianionic dimer $(\mathbf{TCNE})_2^{2-}$, and the neutral dimer $(\mathbf{PHEN})_2$ lies intermediate.

II. Energetics of Dimerization. The distinctive trends of the thermodynamics results in Tables 2−4 as determined by UV−vis and EPR spectral measurements in solution identify six noteworthy features of π-dimerization and the conclusions that can be drawn therefrom as follows.

(i) Those structural factors leading to the diagnostic UV−Vis absorption in π-dimerization equally apply to the electron-pairing properties of the precursor radical as probed by the EPR measurements. The results in Table 2 show that identical thermodynamic parameters (ΔH_D and ΔS_D) derive from the reversible dimerizations (K_D) via the application of two independent methodologies. Thus, the two-electron pairing in the π-bonded dimer also pertains to the intra-dimer electronic HOMO−LUMO transition in Chart 4.[33]

(ii) The magnitudes of both the enthalpy and entropy changes in π-dimerization are relatively constant and independent of the charge on the precursor radical. As such, any repulsive force inherent to intra-dimer electrostatics does not materially affect the stabilization energy of the π-bonded dimer in solution.[34]

(iii) The relatively large negative entropy change is an important contributor to the Gibbs free-energy change in π-dimerization. Moreover, the values of $-\Delta S_D$ for π-dimerization are substantially larger than those $-\Delta S_P$ encountered in pimer formation; for example, $\Delta S_D = -33$ for $(\mathbf{OMB})_2^{2+}$ but $\Delta S_P = -0.5$ for $(\mathbf{OMB})_2^{+\bullet}$, and $\Delta S_D = -36$ for $(\mathbf{PHEN})_2$ but $\Delta S_P = -13$ for $(\mathbf{PHEN})_2^{+\bullet}$, with all units in eu.[35]

(iv) The enthalpy changes in the two-electron π-dimerization are roughly twice as large as those in the formation of the one-electron pimer; for example, $\Delta H_D = -9.5$ for $(\mathbf{PHEN})_2$ but $\Delta H_P = -6.4$ for $(\mathbf{PHEN})_2^{+\bullet}$, and $\Delta H_D = -8.8$ for $(\mathbf{OMB})_2^{2+}$ but $\Delta H_P = -2.9$ for $(\mathbf{OMB})_2^{+\bullet}$, with all units in kcal M^{-1}.[35] Most notably, the large negative enthalpies are responsible for the strong temperature dependence of α_M in Figures 2 and 3 and lead to the preponderance of dimeric forms even at relatively high temperatures.[36]

(v) The thermodynamic parameters (both ΔH_D and ΔS_D) are singularly unaffected by changes in either their size (M_4N^+ versus Bu_4N^+) or the nature of the counterion (Na^+ versus Et_4N^+) in Table 3. It follows that the stability of the dimeric species is not measurably dependent on ion pairing or counterion electrostatics.[34]

(vi) Although the thermodynamic properties of π-bonded dimers are strongly subject to solvent effects, the diagnostic spectral properties (ν_L, ϵ_L) are singularly unaffected in Tables 4 and S2. Thus, large changes in the solvation of the dimeric species can occur without any detectable effect on the dimer *structure*, as evaluated by alteration of the separation parameter d_D.[37]

III. Structural Characteristics of the π-Bonded Dimer. The principal feature of all π-bonded radical/radical dimers, such as those derived from the precursors depicted in Charts 2 and 3, is the cofacial arrangement of the monomeric moieties at interplanar separations d_D that are substantially less than that imposed by van der Waals contact of $d_{vdW} = 3.5$ Å. Such assemblies can lie directly atop one another, as in the tetracyanoethylene dimer $(\mathbf{TCNE})_2^{2-}$ illustrated in Figure 4 and in the phenalenyl dimer $(\mathbf{PHEN})_2$, or they more commonly occur with slight slippage as illustrated for the chloranil dimer $(\mathbf{CA})_2^{2-}$ in Figure 5.[39] Since dimerizations of π-radicals often occur with some distortion from planarity, interplanar measurements are difficult to ascribe precisely, but within 10% deviation, the distance of $d_D = 3.1 \pm 0.3$ Å describes the common interplanar

(30) (a) By comparison, the energy difference Δ in charge-transfer complexes is the principal contributor to the linear Mulliken correlation of the transition energy ($h\nu_{CT}$) with the donor/acceptor redox or ionization potentials. (b) Since H_{ab} has a large contribution from the orbital overlap, its magnitude is generally less in charge-transfer complexes relative to that in π-bonded dimers in which symmetry favors orbital overlap. Consequently, the electronic transitions $h\nu_L$ in π-bonded dimers are comparable to those in related charge-transfer complexes despite the absence of a contribution from the energy difference (Δ = 0). (c) In addition, the increased values of electronic coupling is also reflected in the transition moments of π-bonded dimers, since H_{ab} and log ε are closely related.[29,31] Thus the values of the extinction coefficients of π-bonded dimers lie in the range: $(2-3) \times 10^4$ M^{-1} cm^{-1}, whereas they are typically $(1-10) \times 10^3$ M^{-1} cm^{-1} in charge-transfer complexes.[30d−f] (d) Briegleb, G. *Electronen-Donator-Acceptor Komplexe*; Springer: Berlin, 1961. (e) Foster, R., Ed. *Organic Charge-Transfer Complexes*; Academic: NY, 1969. (f) Foster, R., Ed. *Molecular Complexes*; Crane, Russak: NY, 1973. (g) Creutz, C.; Newton, M. D.; Sutin, N. *J. Photochem. Photobiol. A: Chem.* **1994**, *82*, 47.

(31) The high-energy transition $h\nu_H$ is more difficult to assign with certainty. (a) We suggest that it derives from a charge-transfer transition from the subjacent HOMO-1 (of the dimer) to the LUMO[31c] (see Figure S7). (b) Alternative spectral assignments have been raised by a reviewer who favors the low-energy transition $h\nu_L$ to derive from the charge-transfer transition from HOMO- 1 to LUMO and the high-energy transition from HOMO-2 to LUMO, with HOMO/LUMO and HOMO-2/HOMO-1 splittings roughly comparable. Such an orbital diagram can account for the significant difference experimentally observed between $h\nu_L$ in the dimer and pimer (see Figure 7). However, this alternative predicts an additional low-energy band in the NIR region of the dimer that is roughly comparable to that observed in the pimer. However, careful scrutiny in this region of the electronic spectra has failed to reveal such unmistakable NIR bands. Furthermore, this alternative assignment incorrectly predicts that $h\nu_L$ of the dimer should be the same as the local (HOMO to SOMO) transition $h\nu_M$ in the monomeric species listed in Table 1 (column 3), since $h\nu_M$ is in fact is clearly discrepant from the experimental value of $h\nu_L$ cited in column 6. (c) Note that the consistent blue-shifts of $h\nu_H$ in the dimer relative to $h\nu_M$ in the monomer indicate that the HOMO/LUMO splitting is larger than the HOMO-2/HOMO-1 splitting.

(32) The dimeric unit $(\mathbf{TCNQ})_2^{2-}$ is not included because the dimer spectrum could not be reliably measured in organic solvents. Note that the value of ν_L in Table 1 was obtained in water.[14b]

(33) (a) EPR studies of singlet → triplet transitions of the dimeric forms in solution will be reported separately. For the triplet exciton behavior of $\mathbf{TCNQ}^{-\bullet}$ and $\mathbf{DDQ}^{-\bullet}$ salts in the crystalline solid state, see: (b) Flandrois, S.; Amiell, J.; Carmona, F.; Delhaes, P. *Solid State Comm.* **1975**, *17*, 287. (c) Gordon, D.; Hove, M. J. *J. Chem. Phys.* **1973**, *59*, 3419.

(34) The doubly negative dimeric unit $(\mathbf{TCNE})_2^{2-}$ exists in the crystalline solid state according to Miller and co-workers by virtue of cation-mediated attractive forces imposed by counterions.[4,5] In the absence of such electrostatic attraction, the isolated $(\mathbf{TCNE})_2^{2-}$ dimers as in the gas phase were calculated to be energetically unstable with respect to dissociation. Our thermodynamic measurements in nonpolar solvent to roughly approximate the gas phase do not support this prediction, and electrostatic calculations based on crystallographic data from quite different crystal packings of four separate salts of $(\mathbf{TCNE})_2^{2-}$ indicate that within 3% the interplanar separation of $d_D = 2.90 \pm 0.08$ Å is quite independent of marked variations in the calculated electrostatics; see Table S4.

(35) See: Table S3 in Supporting Information for details.

(36) Entropy changes in the intermolecular formation of charge-transfer complexes generally lie in the range $-\Delta S_{CT} = 5-20$ eu., and corresponding enthalpy changes are generally $-\Delta H_{CT} = 2-10$ kcal mol^{-1}.[28,30]

(37) The direct relationship between the optical (CT) transition and the separation parameter is established by the Mulliken−Hush expression:[28,38] $H_{ab} = 0.0206(\nu_L \Delta\nu_{1/2} \epsilon_L)^{1/2}/d_D$, where ν_L and $\Delta\nu_{1/2}$ are the CT spectral maximum and full width at half-maximum (cm^{-1}), respectively, and ϵ_L is the extinction coefficient (M^{-1} cm^{-1}).

(38) (a) Hush, N. S. *Z. Elektrochem.* **1957**, *61*, 734. (b) Hush, N. S. *Trans. Faraday Soc.* **1961**, *57*, 557. (c) Hush, N. S. *Prog. Inorg. Chem.* **1967**, *8*, 391. (d) Hush, N. S. *Electrochim. Acta.* **1968**, *13*, 005. (e) Creutz, C.; Newton, M. D.; Sutin, N. *J. Photochem. Photobiol. A: Chem.* **1994**, *82*, 47.

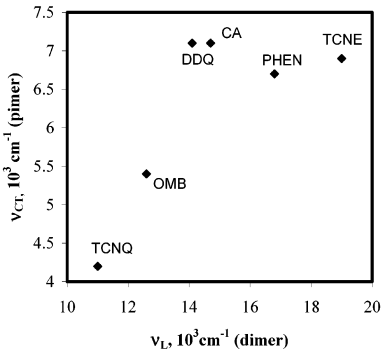

Figure 7. Relationship between the transition energy ν_L of two-electron dimers versus the charge-transfer transition ν_{CT} of the corresponding one-electron pimer, as indicated.

separation in all π-bonded dimers irrespective of whether they exist as doubly charged anions and cations or uncharged units. Further indications of the significant bonding interaction in such dimeric units can be inferred from the angular distortions such as ($\theta = 6.5°$) in $(\mathbf{TCNE})_2^{2-}$ in Figure 4B and the asymmetric bending of $\theta_i = 4.5°$, $\theta_o = 0°$ in $(\mathbf{CA})_2^{2-}$ in Figure 5B. Other examples of planar distortions are observed in π-bonded dimers derived from dichlorodicyanoquinone anion radical[2b,10] and the octamethylbiphenylene cation radical.[12]

IV. Intermolecular Associations of π-Radicals in a Generalized (Charge-Transfer) Context. The energy gain at dimerization derives from electron delocalization via the interacting frontier orbitals over two molecular moieties, as illustrated in Chart 4.[40] In the dimer, two electrons reside on the bonding MO, whereas, in the pimer, the delocalization of a single electron provides the exchange energy for association.[16] The transition energy $h\nu_L$ of the two-electron dimer is generally twice that $h\nu_P$ in the corresponding one-electron pimer, and there is a rough correlation between these, as observed in Figure 7. Since the transition energy is related to the value of the resonance integral H_{ab}, such an observation is consistent with the stronger binding in the dimer relative to that in the one-electron pimer, in line with the higher values of $-\Delta H_D$ relative to $-\Delta H_P$ (Tables 2 and S3), despite the inherent penalty encountered from the electrostatic repulsion in doubly charged dimeric units. This enthalpy gain is compensated by a higher entropy loss in dimerization and leads to a sharper increase of K_D relative to K_P at lower temperature. The latter also accounts for the more facile isolation of dimers relative to pimers at low temperatures. Comparative structural data also indicate that the interplanar separation in the pimer $(\mathbf{OMB})_2^{+\bullet}$ is somewhat higher with $d_P = 3.4$ Å than the corresponding dimer $(\mathbf{OMB})_2^{2+}$ with $d_D = 3.2$ Å, but the difference is nil in $(\mathbf{DDQ})_2^{-\bullet}$ versus $(\mathbf{DDQ})_2^{2-}$ and in $(\mathbf{TCNQ})_2^{-\bullet}$ versus $(\mathbf{TCNQ})_2^{2-}$.[40]

In a more general context, the spectroscopic, thermodynamic, and structural features of π-bonded dimers and pimers bear a strong relationship to those of more conventional charge-transfer complexes derived from wholly diamagnetic precursors comprised of electron-rich donors and electron-poor acceptors,[16] as originally envisaged by Mulliken.[29] Indeed, such a far-reaching conclusion was predicted by Mulliken in a cryptic, insightful comment made more than three decades earlier![41] In the generalized charge-transfer context, π-associations involving a pair of planar π-donors and π-acceptors are strongly subject to steric effects,[42] and the uniform interplanar separation of $d_D = 3.2 \pm 0.2$ Å[30d-f] that pertains to such charge-transfer complexes is essentially the same as that obtained in two-electron dimers and one-electron pimers (vide supra). Viewed in this way, open-shell π-radicals elicit ambivalent behavior as an electron donor or acceptor depending on whether its counterpart is (a) a closed-shell acceptor or donor to form pimers or (b) an open-shell radical to form dimers.[43]

Summary and Conclusions

The combined use of electronic UV−vis and EPR spectroscopic techniques in solution and in solid state, together with rigorous structural measurements by X-ray crystallographic analyses, provide unequivocal evidence for the ubiquitous formation of π-bonded dimers from the spontaneous and reversible association of a pair of charged as well as uncharged planar π-radicals. The diamagnetic dimers are characterized by (a) intense electronic absorption bands that uniformly occur in the near-IR region and (b) interplanar separations of $d_D = 3.05 \pm 0.25$ Å, irrespective of whether the dimeric units bear a double-positive charge or double-negative charge or are overall uncharged.[44] The maximum separation distance in such intermolecular associations is that of the van der Waals limit $d_{vdW} \approx 3.5$ Å for radicals comprised of carbon π-centers. The magnitude of $d_D = 3.05$ Å which is roughly 0.4 Å shorter than the van der Waals contact largely reflects the intra-dimer stabilization energy H_{ab} arising from the π-electron delocalization that is qualitatively depicted in Chart 4 (right). Extra-dimer forces from counterion electrostatics, crystal packing, and so forth inflict rather minor perturbations since the value of d_D is remarkably invariant in (a) various salts anion-radical dimers with a wide range of positively charged counterions,[5] (b) different crystalline stacking arrangements of anion-radical salts, especially those of $\mathbf{TCNQ}^{-\bullet}$, $\mathbf{TCNE}^{-\bullet}$ and $\mathbf{DDQ}^{-\bullet}$,[2,5,10] and (c) dimeric forms measured in solution versus the solid state.[45]

(39) Thus the bending in the dimeric unit $(\mathbf{TCNE})_2^{2-}$ is in accord with the pseudo-"cyclobutanoid" structure of the carbon skeleton, as described by Miller and co-workers.[4,5] Analogously, the bending of the "inner" carbonyl dipoles in $(\mathbf{CA})_2^{2-}$ are symptomatic of an attractive interaction of the carbonyl acceptor with the π-donor property of the juxtaposed (C−C) double bond.

(40) (a) The dimeric nature of the ground state in Chart 4 (right) is open to question. Although it is speculatively presented here as a single (HOMO) orbital containing two electrons, a reviewer has suggested a pair of interacting SOMOs with correlated electron spins, that is, a singlet diradical. (b) An ongoing collaborative program with M. Head-Gordon, Berkeley is aimed at the theoretical quantum mechanical basis for mapping out precise potential-energy surfaces and π-bonding characteristics of the two-electron dimers, with particular regard to their one-electron pimer counterparts. (c) More extensive comparisons with dimer structures are not possible at this juncture owing to the paucity of precise pimer structures arising from inherently weaker one-electron bindings.

(41) See: Mulliken, R. S.; Person, W. B. *Molecular Complexes*. Wiley: NY, 1969; p 40, Table 4-1.

(42) Rathore, R.; Lindeman, S. V.; Kochi, J. K. *J. Am. Chem. Soc.* **1997**, *119*, 9393.

(43) (a) In the latter context, π-dimerization can equally well result from the π-associations of various combinations of diamagnetic cation/anion dyads. (b) Other generalized examples of such paramagnetic associates are the transient CT complexes of halogen atoms ($Cl^{\bullet}$, $Br^{\bullet}$, and $I^{\bullet}$ as electron acceptors) with arene donors. For example, see: Raner, K. D.; Lusztyk, J.; Ingold, K. U. *J. Phys. Chem.* **1989**, *93*, 564 and references therein.

(44) The marked invariance of the separation parameter d_D for the dimeric structure despite large differences in the homosoric/heterosoric stackings of the radical units is further indication of its structural integrity.

(45) The direct relationship between the charge-transfer transition in solution and in the crystalline solid state is illustrated in Figure 6. Note that the slight red-shift in the solid-state spectra has been previously noted. See: Oohashi et al. in ref 24b, Itoh in ref 14c, Sakai et al. in ref 14k, and Miller et al. in ref 5.

The intrinsic stability of π-dimers derives from relatively high values of the enthalpy change with $-\Delta H_D$ in the range 6−10 kcal mol^{-1} which are compensated by large entropy changes of $-\Delta S_D$ in the range 25−40 eu in Table 2. Despite the rather modest equilibrium constants at room temperature, the large enthalpy change leads to their sharp increase at lower temperatures in Figures 2 and 3. Comparative spectroscopic, thermodynamic, and structural analyses (Tables 2 and S3) underscore the direct relationship between the two-electron radical/radical dimers and the analogous one-electron pimers in Figure 7 to the more conventional charge-transfer complexes derived from planar diamagnetic donor/acceptor dyads in which there is extensive electron delocalization between a pair of molecular moieties.[46] We believe that the electron delocalizations in both the diamagnetic two-electron and the paramagnetic one-electron π-binding in Chart 4 also have direct relevance to extended systems, particularly those encountered in the vertical and oblique stacking of planar (radical/acceptor) units in the solid state for organic material science.[33b,47] Especially important to the understanding of the magnetic/electric properties of such assemblies is the identification of the electronic coupling element in and between each binary building unit insofar as it is revealed by various separation distances, orientations, and intrinsic donor/acceptor properties.

Experimental Section

Materials. The electron acceptors tetracyanoquinodimethane (**TCNQ**), dichlorodicyanoquinone (**DDQ**), tetracyanoethylene (**TCNE**) and chloranil (**CA**) from Aldrich were purified by repeated recrystallization and/or sublimation in vacuo. Sodium iodide, lithium iodide, tetra-*n*-butyl-, tetra-*n*-propyl-, tetraethyl-, and tetramethylammonium iodides (Acros) were used as received. The anion-radical salts were prepared by the reduction of the neutral acceptors with a 1.5 to 3 molar excess of the corresponding alkali metal or alkylammonium iodide.[16] Bu_4N^+**TCNQ**$^{+\bullet}$ and Bu_4N^+**CA**$^{+\bullet}$ were isolated after ion-exchange of the corresponding alkali-metal salts.[16] 1,2,3,4,5,6,7,8-Octamethylbiphenylene and its cation-radical salts (**OMB**$^{+\bullet}SbCl_6$) were synthesized by procedures described in the literature.[12] 2,5,8-tributylphenalenyl radical **PHEN**$^\bullet$ was similarly prepared by the literature procedure.[11] The sterically hindered radical cation of 9,10-dimethoxy-1,4:5,8-dimethano-1,2,3,4,5,6,-7,8-octahydroanthracene (**CRET**$^{+\bullet}$) was prepared as the $SbCl_6^-$ salt by the literature procedures.[48] Acetonitrile, dichloromethane, acetone, hexane, propionitrile, and butyronitrile were purified according to standard laboratory procedures.[49] All solvents were stored in Schlenk flasks under an argon atmosphere.

X-ray Crystallography. The intensity data were collected with a Siemens SMART diffractometer equipped with a 1 K CCD detector using Mo Kα radiation (λ = 0.71 073 Å) at −150 °C. The structures were solved by direct methods[50] and refined by full matrix least-squares procedure with IBM Pentium and SGI O_2 computers. Note that the X-ray structure details presented here are on deposit and can be obtained from the Cambridge Crystallographic Database.

$[TCNE_2]^{2-}(Bu_4N^+)_2$. A 100-ml flask equipped with a Schlenk adapter was charged with 40 mg of **TCNE**$^{-\bullet}Bu_4N^+$ and 10 mL of dichloromethane was added under argon atmosphere. After dissolution, the solution was covered with hexane and put into a cold (−70 °C) bath. Red-brown crystals of $[\mathbf{TCNE_2}]^{2-}(Bu_4N^+)_2 2CH_2Cl_2$ were formed during 3−5 days and handled at low temperature.

$[CA_2]^{2-}(Pr_4N^+)_2$. A 100-mL flask equipped with a Schlenk adapter was charged with 40 mg (about 0.1 mmol) of **CA**$^{-\bullet}Pr_4N^+$, and 10 mL of dichloromethane was added under argon atmosphere. After dissolution, the solution was covered with a layer of hexane, and the mixture was placed in a cold (−70 °C) bath. Red-brown crystals of $[\mathbf{CA}_2]^{2-}(Pr_4N^+)_2$ formed during 3−5 days.

$[TCNE_2]^{2-}(Bu_4N^+)_2\ 2CH_2Cl_2$. Formula: $C_{24}H_{40}Cl_4N_{10}$. M 1080.82, monoclinic $P2_1/c$, a = 13.878(2) Å, b = 14.381(1) Å, c = 16.120(2) Å, β = 114.33(1)°, V = 2931.5 (7) Å^3, D_c = 1.224 g cm^{-3}, Z = 2. The total number of reflections measured were 17 708 of which 8441 reflections were symmetrically nonequivalent. Final residuals were $R1$ = 0.053 and $wR2$ = 0.141 for 6318 reflections with $I > 2\sigma(I)$.

$[CA_2]^{2-}(Pr_4N^+)_2$. Formula: $C_{36}H_{56}Cl_8N_2O_4$. M 864.42, orthorombic *Pbca*, a = 16.207(1) Å, b = 12.841(1) Å, c = 20.209(1) Å, V = 4205.9 (4) Å^3, D_c = 1.365 g cm^{-3}, Z = 4. The total number of reflections measured were 46 553 of which 7026 reflections were symmetrically nonequivalent. Final residuals were $R1$ = 0.041 and $wR2$ = 0.090 for 4973 reflections with $I > 2\sigma(I)$.

EPR measurements were performed on a Bruker ESP-300 X-band spectrometer with 100 kHz field modulation, 2 G modulation amplitude, and 20 mW microwave power. The radical samples were prepared in a Schlenk tube and transferred under an argon atmosphere into a quartz 2-mm diameter EPR tube connected to a 5-mL Pyrex tube equipped with a Teflon valve. The tube was placed in a quartz Dewar set in the center of a rectangular cavity, and the temperature was regulated by an IBM temperature control unit to within ±0.5 K. Compressed nitrogen was guided through the cavity to remove any adventitious moisture condensed onto the Dewar surface at low temperature.

The intensity of the EPR signals at each temperature, I_{EPR}, was determined by double integration with an uncertainty of 10% of the averaged spectra from five measurements to enhance the signal-to-noise ratio, after baseline correction, and was found to be proportional to the concentration of the radical in the sample (c_M); according to the Curie law to $1/T$, $I_{EPR} = a \times c_M/T$, where a is the proportionality factor.[15] The ratio of the EPR intensities at temperatures T(I_{ESR}) to those at T = 298 K (I_{EPR}^{298}) was expressed as $(I_{EPR}/I_{EPR}^{298}) = (c_M/c_M^{298}) \times (298/T) \times (a/a^{298})$. Note, that the ratio a/a^{298} is included in the expression, since a depends on instrumental parameters, for example, cavity Q-factor, and varies somewhat with temperature. Therefore, to accurately determine c_M/c_M^{298} from the intensity measurements (I_{EPR}/I_{EPR}^{298}), it was necessary to take into account the effects of the Curie low and the variation of a, that is, the factor $(298/T) \times (a/a^{298})$. The latter was determined (for all solvents and temperatures) from the measurements of the EPR intensity of the stable (sterically hindered) radicals **CRET**$^{+\bullet}$ and **DPPH**$^\bullet$ since these radicals do not dimerize (as confirmed by the UV−vis spectroscopy). [Results for both species were essentially the same.] Therefore, $c_M/c_M^{298} = 1$ over the entire temperature range, and variations of the EPR intensities were determined by Curie law plus instrumental factors: $I_{EPR}/I_{EPR}^{298} = (298/T) \times (a/a^{298}) = b^T$. The latter, b^T, is the normalization factor at temperature T. In other words, when the radical's concentration in the sample was constant, the multiplication of intensity ratio I_{EPR}/I_{EPR}^{298} by $1/b^T$ was unity.

For the anion, cation, and neutral radicals derived from precursors in Charts 2 and 3, the normalized values of I_{EPR}/I_{EPR}^{298} (multiplied by corresponding $1/b^T$) were essentially constant (unity) at room temperature and at moderately low temperatures (300−250 K). The latter indicated that the equilibria as in eq 1 were shifted to the left, and monomer concentrations (c_M) were equal to the initial concentration of the radicals salts (c_0); that is, the monomer fraction was unity: $\alpha = c_M/c_0 = 1$.[15] Further lowering the temperatures resulted in a substantial decline of the normalized ratio of the intensity values. Because the

(46) For example, compare: Rosokha, S. V.; Kochi, J. K. *J. Am. Chem. Soc.* **2001**, *123*, 8985.
(47) For example, see: (a) Farges, J.-P., Ed. *Organic Conductors: Fundamentals and Applications*; Marcel Dekker: NY, 1994. (b) Lahti, P. M., Ed.; *Magnetic Properties of Organic Materials*; Marcel Dekker: NY, 1999. (c) Miller, J. S., Drillon, M., Eds. *Magnetism: Molecules to Materials*; Wiley-VCH: Weinheim, 2001.
(48) Rathore, R.; Kochi, J. K. *J. Org. Chem.* **1995**, *60*, 4399.
(49) Perrin, D. D.; Armagero, W. L.; Perrin, D. R. *Purification of Laboratory Chemicals*, 2nd ed.; Pergamon: NY, 1980.
(50) Sheldrick, G. M. *SHELXS-86, Program for Structure Solution*; University of Gottingen: Germany, 1986.

Curie law effects plus instrumental factors were already taken into account, the decrease represented the change in free radical concentration, c_M. Since the decrease of intensity was reversible and became more pronounced at increased initial concentrations, c_0, it was related to formation of diamagnetic dimers.[15] The quantitative treatment of the EPR intensity data, together with electronic spectroscopy and solid-state data, confirms such an assignment. Accordingly, the measurements of EPR intensity led to the monomer fraction at different temperatures: $\alpha = I_{EPR}/I_{EPR}^{298} \times (1/b^T)$. The latter allowed the calculation of the equilibrium constant: $K_D = (1 - \alpha)/2c_0\alpha^2$.[15] Finally, the thermodynamic parameters for dimerization were calculated by the least-squares procedure from the linear dependence of ln K_D with $1/T$ as measured at different radical concentrations (Figure 3 and Table 1).

UV measurements were carried out on an HP 8453 diode-array spectrophotometer in a Dewar equipped with quartz lens, and the temperature was adjusted with an ethanol−liquid nitrogen bath (±0.5 K). The radical samples for the UV−vis measurements were prepared in a Schlenk tube and transferred under an argon atmosphere into the quartz (1-mm path length) spectroscopic cell equipped with a Teflon valve fitted with Viton O-rings. The samples of radical salts (KBr pellets or Nujol oil) for solid-state UV−vis absorption measurements were prepared under an argon atmosphere in a glovebox. The blue solution of octamethylbiphenylene cation-radical **OMB**$^{+\bullet}$ (prepared as crystalline $SbCl_6^-$ salt) in dichloromethane at 25 °C showed the characteristic absorption spectrum with a band centered at 602 nm (λ_M) and a minor satellite at 555 nm.[12a] The intensity of λ_M at room temperature was strictly proportional to the initial concentration of the cation-radical salt, and at the low concentration of ∼0.1 mM, the shape of the spectrum was essentially temperature independent. The close scrutiny of the spectra of **OMB**$^{+\bullet}$ at higher concentrations of >1 mM indicated the appearance of the new low-intensity bands at ∼790 and 500 nm (λ_L and λ_H). These band intensities increased substantially with the lowering of the temperature, and their growth was accompanied by the decrease of λ_M (Figure 1). The temperature-dependent spectral changes observed for dichloromethane solutions of **OMB**$^{+\bullet}SbCl_6^-$ were quite reversible, and the existence of the clear isosbestic points in Figure 1A indicated the quantitative interchange between two absorbing species. Importantly, the intensity of λ_H at constant temperature was proportional to the square of the concentration of **OMB**$^{+\bullet}SbCl_6^-$ (Figure S1). Such concentration and temperature dependencies indicated the reversible equilibrium in eq 1 between monomeric (λ_M) and dimeric (λ_L and λ_H) forms of the octamethylbiphenylene cation radical. This conclusion was supported by the quantitative treatment of the UV−vis spectral changes in Figure 2 and independently by the EPR spectral studies in Table 2 and Figure 3 and the solid-state X-ray crystallography together with the electronic spectroscopic data in Figure 7. The same analysis of the concentration and temperature dependence of spectral changes was applied to the neutral phenalene radical **PHEN**$^\bullet$ and to the π-dimerization of the anion radicals of π-acceptors. Thus, the extinction coefficients ϵ_M of the monomeric cation, anion, and neutral radicals were measured at room temperature in the concentration range $c_0 = 0.1-0.5$ mM. Under such conditions, the dimer formation was negligible, and the absorption intensity was proportional to c_0. Therefore, extinction coefficients ϵ_M in Table 1 were calculated directly from the intensity of absorption at λ_M; the values agreed with the literature data for all the radicals studied. The extinction coefficients ϵ_L for $(\mathbf{OMB})_2^{2+}$ and $(\mathbf{DDQ})_2^{2-}$ dimers were determined from the temperature-modulated spectral changes (Figure 1), in which the decrease of absorbance at λ_M (ΔA_M) upon lowering the temperature was linearly related to the absorbance increase at λ_L (ΔA_L). Therefore, ϵ_L was calculated as $\epsilon_L = -(2\epsilon_M - \epsilon_D^M) \times \Delta A_L/\Delta A_M$. Note that (i) the absorption of the monomer at λ_L is negligible and (ii) the residual absorption of dimer ϵ_D^M at the monomer band maximum λ_M, as calculated by step-by-step approximations (see Supporting Information), and (iii) apparent changes in concentrations due to the volume changes with temperature were taken into account to ensure accuracy. Based on the values of ϵ_L, the concentration of dimer c_D was calculated at different temperatures, and c_0, from the absorption intensity at λ_L, which led to the monomer fraction $\alpha = (c_0 - 2c_D)/c_0$ and equilibrium constant $K_D = (1 - \alpha)/2c_0\alpha^2$. Finally, the thermodynamic parameters for dimerization (Table 1) were calculated by the least-squares procedure from the linear dependence of ln K_D on $1/T$ measured at different values of c_0. The reliability of these values was confirmed by independent calculations of K_D from the intensity of the monomer absorption band λ_M and by comparison with the EPR-based values. For the radical anions **TCNE**$^{-\bullet}$ and **CA**$^{-\bullet}$, the dimer bands λ_L were observed only at very low temperatures in highly concentrated solutions with $c_0 = 5-10$ mM. Under these conditions, the monomer absorptions at λ_M were too high to be measured (Figures S2 and S3). For **PHEN**$^\bullet$, the weak band at λ_M ($\epsilon_{545} = 103$ M^{-1} cm^{-1}) was overshadowed by the dimer absorption (Figure S4). Accordingly, for these three radicals, the simultaneous measurement of the monomer intensity and the dimer absorption bands for use by the methodology described above was precluded. Therefore, the extinction coefficients ϵ_L and thermodynamic parameters for dimerization (ΔH_D, ΔS_D) were calculated by an approximation method based on the measurement of the intensity of the absorption of a pure dimer band with a maximum at λ_L. The procedure included the variation of the extinction coefficient and the thermodynamic parameters to minimize the difference between the experimental and calculated values of the absorption at λ_L: $\Delta = \Sigma(A^i_{exp} - A^i_{calc})^2$. Experimental values of A^i_{exp} were measured at different temperatures and initial concentrations; $A^i_{calc} = \epsilon_L \times l \times c_D = \epsilon_L \times l \times [(4K_D \times c_0 + 1) - (8K_D \times c_0 + 1)^{0.5}]/8K_D$, with $K_D = \exp[-(\Delta H_D - T\Delta S_D)/RT]$ and $l = 0.1$ cm. The reliability of the procedure was confirmed by comparison of the extinction coefficients of anion-radical dimers with those values available in the literature[14c,k] and the thermodynamic parameters to those calculated from ESR measurements. Spectral overlap, together with the very high intensity of absorption band of **TCNQ**$^{-\bullet}$ monomer around 800 nm, prevented the accurate calculation of the thermodynamic parameters for dimerization in dichloromethane solutions based on spectrophotometric measurements.

Acknowledgment. We thank J. H. Kim and V. Ganesan for initial observations of $(\mathbf{OMB})_2^{2+}$, $(\mathbf{TCNQ})_2^{2-}$, and $(\mathbf{DDQ})_2^{2-}$; D.L. Sun for the first isolation of the crystalline salts of $(\mathbf{CA})_2^{2-}$; V. Zaitsev for the data in Tables 1 and 2 (to be published with M. Head-Gordon[40b]) of the phenalenyl radical **PHEN**$^\bullet$; and S. V. Lindeman for invaluable crystallographic assistance. We also thank the R. A. Welch Foundation and National Science Foundation for financial support.

Supporting Information Available: Equilibria constants of dimer formation K_D at +25 and −80 °C (Table S1), solvent effects on spectral characteristics of the $(\mathbf{DDQ})_2^{2-}$ dimer and thermodynamics of its formation (Table S2), spectral characteristics of pimers and thermodynamics of their formation (Table S3), concentration dependence of absorbance at λ_L (Figure S1), electrostatics effects in the $(\mathbf{TCNE})_2^{2-}$ dimer formation (Table S4), details of the dimer (UV−vis) spectral characterization, temperature modulated spectral changes in the solutions of **TCNE**$^{-\bullet}$, **CA**$^{-\bullet}$, and **PHEN**$^\bullet$ (Figures S2−S4), temperature dependence of monomer fraction (EPR measurements) in the solution of **TCNQ**$^{-\bullet}$ and **DDQ**$^{-\bullet}$ (Figures S5 and S6), molecular orbital diagram for dimers (Figure S7). This material is available free of charge via the Internet at http://pubs.acs.org.

JA0364928